SPECIAL ISSUE ARTICLE

Journal
American Ceramic Society

Digital light processing stereolithography of hydroxyapatite scaffolds with bone-like architecture, permeability, and mechanical properties

Francesco Baino[1] | Giulia Magnaterra[1] | Elisa Fiume[1,2] | Alessandro Schiavi[3] | Luciana-Patricia Tofan[4] | Martin Schwentenwein[4] | Enrica Verné[1]

[1]Department of Applied Science and Technology (DISAT), Politecnico di Torino, Turin, Italy

[2]Department of Mechanical and Aerospace Engineering (DIMEAS), Politecnico di Torino, Turin, Italy

[3]Applied Metrology and Engineering Division, National Institute of Metrological Research (INRiM, Turin, Italy

[4]Lithoz GmbH, Vienna, Austria

Correspondence
Francesco Baino, Department of Applied Science and Technology (DISAT), Politecnico di Torino, 10129 Turin, Italy.
Email: francesco.baino@polito.it

Abstract

This work deals with the additive manufacturing and characterization of hydroxyapatite scaffolds mimicking the trabecular architecture of cancellous bone. A novel approach was proposed relying on stereolithographic technology, which builds foam-like ceramic scaffolds by using three-dimensional (3D) micro-tomographic reconstructions of polymeric sponges as virtual templates for the manufacturing process. The layer-by-layer fabrication process involves the selective polymerization of a photocurable resin in which hydroxyapatite particles are homogeneously dispersed. Irradiation is performed by a dynamic mask that projects blue light onto the slurry. After sintering, highly-porous hydroxyapatite scaffolds (total porosity ~0.80, pore size 100-800 µm) replicating the 3D open-cell architecture of the polymeric template as well as spongy bone were obtained. Intrinsic permeability of scaffolds was determined by measuring laminar airflow alternating pressure wave drops and was found to be within $0.75\text{-}1.74 \times 10^{-9}\,\text{m}^2$, which is comparable to the range of human cancellous bone. Compressive tests were also carried out in order to determine the strength (~1.60 MPa), elastic modulus (~513 MPa) and Weibull modulus ($m = 2.2$) of the scaffolds. Overall, the fabrication strategy used to print hydroxyapatite scaffolds (tomographic imaging combined with digital mirror device [DMD]-based stereolithography) shows great promise for the development of porous bioceramics with bone-like architecture and mass transport properties.

KEYWORDS
additive manufacturing, bone tissue engineering, hydroxyapatite, porosity, scaffold

1 | INTRODUCTION

Bone tissue is able to self-regenerate, but, in the presence of large defects due to trauma, tumor removal or congenital diseases, surgical insertion of a bone graft is needed to promote a faster and effective tissue healing. It was estimated that more than 2 million people worldwide annually undergo bone surgery to repair critical osseous defects.[1] At present, both biological (i.e. transplant materials) and synthetic grafts are used. The latter option is usually preferred in modern bone

---

tissue engineering approaches as the use of man-made bio-materials allows overcoming the problems of transplant tissue shortage, immune compatibility/rejection, and the need for harvesting extra-surgery in the case of autologous grafts.[2]

Synthetic bone grafts are often produced in the form of three-dimensional (3D) porous structures (scaffolds) that are able to form a strong bond to bone tissue.[3] Scaffolds must exhibit high and interconnected porosity, provide structural support to host tissue and withstand the physiological loads while promoting cell adhesion and growth along with vascularization, thus leading to new bone regeneration.[4]

Among bioceramics, synthetic hydroxyapatite is highly suitable to fabricate bone scaffolds due to its compositional and crystallographic similarity to bio-apatite, which constitutes more than 60% of the inorganic bone matrix.[5] Its significance in biomedicine and biomaterials science has been widely demonstrated over more than 50 years of clinical use in orthopedics.[6]

Hydroxyapatite-based porous scaffolds (both full-ceramic and composite) have been manufactured by several technologies, ranging from the traditional ones, that is, foam replication,[7,8] dry process with porogen agents[9] and isostatic pressing without sintering,[10] to the latest solid free-form (SFF) fabrication strategies.[11]

Among traditional methods, foam replication shows several advantages including the high versatility, which allows the production of irregularly-shaped bone like products with various pore features, no need for toxic chemicals and the very low cost of implementation, making it a technology with a high commercialization potential. However, foam replication is highly operator-dependent, poorly reproducible and standardized, thus being suitable in just a minority of clinical applications.

Despite the higher technological costs, additive manufacturing technologies have recently shown great promise to produce bioceramic scaffolds, including porous hydroxyapatite, allowing an accurate control on internal pore and strut features to be achieved.[12] In this regard, lithography-based methods allow obtaining high-quality ceramic products with the best spatial resolution among the currently-available rapid-prototyping techniques (less than 50 μm). The latest evolution of stereolithographic methods is based on digital light processing (DLP), which relies on a dynamic mask to promote the polymerisation of a complete layer of photocurable resin gluing the ceramic particles per irradiation cycle. Compared to other stereolithographic methods, this bottom-up approach actually carries some advantages. First of all, photo-cured layers are no longer immersed in the slurry, and this reduces not only the amount of material required but also the risk of introducing defects during the layer-wise building of the product.[13] Moreover, regardless of the shape, size and complexity of the final products, production times are drastically reduced, thereby carrying obvious advantages from economic and technological viewpoints, which are key when mass production is required and/or just partially stable resins are used that need fast processing times.[14]

Another strength of this approach is the great geometrical fidelity that comes with the additive layer-by-layer approach allowing design-oriented production instead of production-oriented design. This advantage is also highlighted by the geometrically extremely-complex test design produced that was used in the course of the present study.

Like most additive manufacturing techniques applied to bone scaffolds, DLP-based stereolithography aims at layerwise reproducing a virtual model which typically derives from (i) computer-built geometries based on repetitive geometrical elements such as unit cells (eg, grid-like structures) that, however, are unable to properly replicate the trabecular architecture of cancellous bone, or (ii) medical reconstructions of patient's bone, which may be more difficult to acquire and/or use as input files (problems of compatibility between medical file type and printing apparatus). Moreover, another issue with the latter approach is the large file size that comes with precise approximations of naturally occurring stochastic cellular/tissue designs.

In order to overcome these limitations, the present study reports, for the first time, the use of a tomographic reconstruction of an open-cell polymeric foam as an input file to the DLP-based stereolithographic system. Polymeric sponges are indeed highly suitable templates for scaffolding since they have been used for many years in the production of bone-like glass and ceramic scaffolds by the conventional sponge replica method due to their similarity with the trabecular architecture of cancellous bone.[15]

2 | EXPERIMENTAL PROCEDURES

2.1 | Preparation of scaffolds

2.1.1 | Slurry

A photocurable slurry named LithaBone HA 480 E (Lithoz, Austria) was used for the present study. The slurry, designed and produced by Lithoz, comprises hydroxyapatite powder and a photocurable binder matrix containing solvent, reactive monomers based on acrylates and methacrylates, and photoinitiator.

2.1.2 | Printing system

Scaffolds were fabricated by using the CeraFab 7500 system that employs the DLP-based stereolithographic method. This system is highly effective for the manufacturing of complex

3D ceramic structures and uses a LED light source in the blue range of the electromagnetic spectrum (wavelength 460 nm). The light engine utilizes powerful LEDs as a light source and a digital mirror device (DMD) chip as a dynamic mask with a resolution of 1920×1080 pixels and a pixel size of 40×40 μm^2.[16]

The DMD chip of CeraFab 7500 system enables a spatially selective photopolymerization of each layer; the resolution in the x–y plane is 40 μm and the thickness of a single layer can in the range of 25 to 100 μm, depending on the user's choice; specifically, the layer thickness used in this work was 25 μm. During printing, the light source radiates from below the rotating vat that is uniformly filled with slurry (bottom-up approach). When the photosensitive suspension is irradiated by external blue light, free radicals are formed and polymerization can take place. As a result, the ceramic particles are bonded in the desired pattern by the polymer, acting as glue between them.

2.1.3 | Scaffold design and manufacturing

In order to obtain 3D porous scaffolds closely resembling the architecture of cancellous bone, a computer-aided design (CAD) file created from micro-computed tomography (micro-CT) of a 45-ppi commercial polyurethane sponge was used as the input to the printing system after being converted to STL extension. The average pore size of the porous template, assessed in a previous study by micro-CT imaging,[17] was 580 μm, which is compatible with the typical reference range reported for trabecular bone.

DLP stereolithography was used to carry out the printing process, thus allowing to faithfully reproduce the selected design, while InVesalius software, widely appreciated in various fields of engineering, archaeology and industrial applications as well as in medicine to assist physicians for diagnosis and surgical planning,[18] was used for the processing of the CAD file describing the structural features of the polymeric template. The InVesalius software allowed reconstructing the 3D profile of the polymeric sponge starting from 771 2D image (.bmp) files, thus obtaining an almost cubic 3D structure for scaffold printing ($4.72 \times 5.15 \times 5.00$ mm; total porosity of 81.8 vol%).

In order to obtain scaffolds with similar size and geometry to commercial hydroxyapatite products, like Endobon®,[19] it was decided to fabricate samples with cylindrical shape and length-to-diameter ratio (aspect ratio) of 2:1. This was possible by joining an exact and overturned copy of the sponge structure to the original cuboid from micro-CT imaging, thus obtaining a parallelepiped; then, the circle inscribed on the squared base was considered in order to extrapolate a cylinder with diameter of 5 mm and height of 10 mm. This process is displayed in Figure 1.

In order to ensure successful printing and mechanical integrity of the 3D scaffolds, both scaling (+25%) and contouring operations (contouring offset = +25 μm) were performed on the original STL file during the creation and tuning of the CAD model. This was useful to increase the thickness of the struts in the greens and limit their breakage upon printing and/or cleaning procedures.

The STL data corresponded to file sizes between 80 and 500 MB for an individual part, or multiples if more than one part was printed simultaneously in one run.

Before printing, the surface of the building platform was coated with a special LithaFoil sheet (Lithoz, Austria) which is a thin layer of thermoplastic polymer foil to increase adhesion between the building platform and the first layer created. Eighteen cylindrical scaffolds were produced simultaneously over a complete printing cycle.

In order to obtain scaffolds with final dimensions close to the nominal ones, shrinkage compensation factors equal to 1.206 along the x, y axes and 1.250 along the z axis were applied (oversizing of green samples).

2.1.4 | Post-processing and sintering

After being printed, green samples were removed from the building platform by using razor blades and carefully cleaned by a cleaning agent and pressurized air in order to eliminate the uncured slurry from the micrometric cavities. Cleaned green samples were then stored at 42°C for no longer than 5 days and thermally treated in an electrical furnace (Nabertherm P330) to completely remove the organic binder and sinter the ceramic particles. As shown in Figure 2, a multistep and slow thermal treament was applied, thus avoiding the formation of internal stresses resulting from gases formed during the polymer burn-off. The thermal post-processing protocol was developed on the experience of slurries which were based on the same
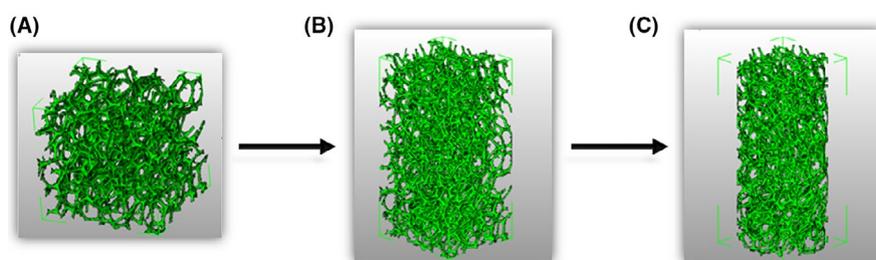

FIGURE 1 STL files visualized in Autodesk Netfabb Premium 2019. (A) cubic sponge; (B) "doubled" cubic sponge; (C) final cylindrical structure with aspect ratio of 2:1
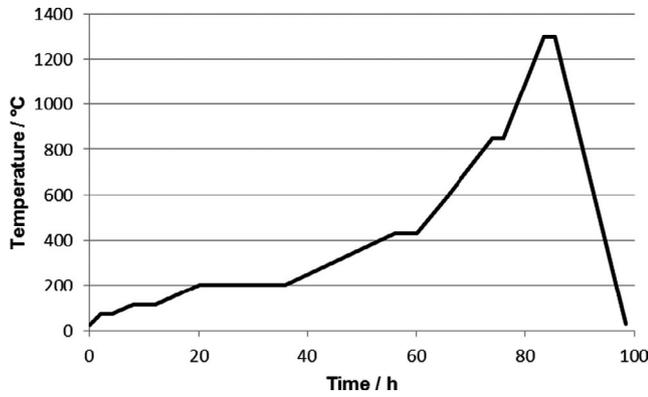
FIGURE 2 Thermal treatment used to consolidate (binder burn-off and sintering) bioceramic scaffolds

basic binder system in Lithoz.[20] The total treatment time was 99 hours (about 4 days); a maximum temperature of 1300°C was reached and mantained for about 2 hours. An auxiliary paste (IPS Object Fix Flow) was used to stabilize and fix the samples to the supporting platform in the furnace; the paste was then easily removed once the sintering process was completed.

2.2 | Characterizations

2.2.1 | Microstructural and morphological analysis

After being crushed in powder, the scaffolds underwent wide-angle (2θ within 10-70°) X-ray diffraction (XRD) by using a X'Pert Pro PW3040/60 diffractometer (PANalytical, Eindhoven, The Netherlands) in order to identify the crystalline phase(s). Working parameters were voltage 40 kV and current 30 mA; setup included Bragg-Brentano camera geometry with Cu Kα incident radiation (wavelength $\lambda = 0.15405$ nm), step size of 0.02° and counting time of 1 second per step. Phase identification was carried out by using X'Pert HighScore software (2.2b) equipped with the PCPDFWIN database.

After being sputter-coated with a thin layer of chromium (10 nm), intact scaffolds were inspected by scanning electron microscopy (SEM; JCM 6000Plus Versatile Benchtop SEM, JEOL).

2.2.2 | Assessment of permeability

At the macroscale level for laminar flows, the proportional relationship between the pressure drop gradient and the fluid volumetric flow rate is described by the Darcy's law[21-23] in its empirical form (Equation (1)):

$$\frac{\Delta P}{L} = \frac{\mu}{k} \cdot \frac{Q_v}{A} \tag{1}$$

where ΔP is the pressure differential upstream and downstream the porous material along the length L of the sample, μ is the dynamic viscosity of the fluid, k is the intrinsic Darcian permeability, Q_v is the volumetric flow rate, and A is the cross-sectional area of the sample perpendicular to the flow direction.

In this work, the intrinsic Darcian permeability k was experimentally determined by measuring the pressure wave drop of a slow alternating airflow,[24-26] with a known volumetric airflow rate through the scaffold, according to Equation 2:

$$k = \mu \frac{q_{v,rms}}{p_{rms}} \cdot \frac{L}{A} \tag{2}$$

where $q_{v,rms}$ was the root-mean-square (r.m.s.) value of alternating volumetric airflow rate, that is, $q_{v,rmsm} = \omega \partial V \cdot \frac{1}{\sqrt{2}}$, depending on the imposed angular frequency of oscillation ω and the corresponding volume variation ∂V within a given volume of air V_0; and p_{rms} was the r.m.s. value of the occurring sinusoidal pressure component, ie $p_{rms} = \gamma p_0 \partial V \left(\frac{1}{V_0 \sqrt{2}} \right)$, depending on the atmospheric static pressure p_0 (with heat capacity ratio $\gamma = 1.4$) and the volume variation ∂V, with respect to the volume of the air V_0. The amplitude of the sinusoidal pressure component was measured by a proper capacitive microphone, with a given sensitivity in mV/Pa; the measurement device and the experimental procedure were previously described in detail elsewhere.[24]

Therefore, by combining the quantities above described, the experimental intrinsic Darcian permeability k was obtained by the following physical model (Equation (3)):

$$k = \mu \frac{\omega V_0}{\gamma p_0} \cdot \frac{L}{A} \cdot \zeta \tag{3}$$

where ζ is the experimental ratio between the microphone sensitivity (in mV/Pa) and the corresponding microphone indication (in mV/Pa) of the pressure wave drop amplitude during the compression and rarefaction ∂V of the air volume V_0 through the scaffold under investigation.

According to Darcy's law,[24,26,27] a very low frequency of oscillation ($\omega \approx 1$ rad/s) was imposed to keep the laminar regime of the volumetric airflow rate. Once the quantities in Equation (3) have been assessed, the intrinsic Darcian permeability k of the scaffolds was determined from experimental measurements performed on six different samples (diameter 4.99 ± 0.13 mm, height 9.88 ± 0.09 mm).

2.2.3 | Mechanical properties

The compressive strength of scaffolds (σ) was determined as the ratio F/A by crushing tests, where F was the maximum load registered during the test and A was the initial cross-sectional area. Mechanical tests were performed by using

an MTS System Corp. apparatus (5-kN cell load, cross-head speed 1 mm/min).

The elastic modulus was determined from the linear region of the stress-strain curve.

The total porosity of each scaffold was assessed by mass-volume measurements as $p = (1 - \rho/\rho_0)$, where ρ is the apparent density of the sample (mass-to-volume ratio) and ρ_0 is the bulk density of hydroxyapatite.

Values of porosity, compressive strength, and elastic modulus were expressed as average $\pm$ standard deviation calculated on 23 scaffolds. Dimensions of samples were assessed by a digital calliper: diameter 5.01 ± 0.10 mm, length 10.29 ± 0.13 mm.

The Weibull modulus m of the scaffolds was determined following the procedures described in ASTM C1239-07,[28] which also recommends the testing of at least 20 specimens to obtain reliable results. Specifically, the data from compressive tests were fitted through the Equation (4):

$$\ln\left(\ln\left(\frac{1}{1-P_f}\right)\right) = m\ln\left(\frac{\sigma}{\sigma_0}\right) = m\ln(\sigma) - m\ln(\sigma_0) \quad (4)$$

where P_f was the probability of failure at a stress σ and σ_0 was the Weibull scale parameter.

Thus, a plot of $\ln\left(\ln\left(\frac{1}{1-P_f}\right)\right)$ vs. $\ln(\sigma)$ followed by linear regression gives a straight line of slope m.

The probability of failure P_f was estimated as $(j - 0.5)/N$, where N is the total number of scaffolds tested and j is the specimen rank in ascending order of failure stresses.

Compressive tests were also performed on scaffolds after immersion in simulated body fluid (SBF), which was prepared according to the Kokubo's protocol,[29] for 14 days (five scaffolds) and 1 month (five scaffolds). This solution mimics the composition of human plasma and is commonly used for in vitro testing of biomaterials.[30] A mass-to-volume ratio (scaffold/solution) of 1.5 mg/ml was used, according to common testing protocols.[31] The samples were kept at 37°C in an orbital shaker incubator (IKA 3510001 KS 4000 I Control Incubator Shaker, IKA-Werke GmbH & Co. KG, Staufen, Germany) with a constant shaking speed of 100 rpm over the whole immersion period.

3 | RESULTS AND DISCUSSION

In the present study, trabecular-like hydroxyapatite scaffolds for bone repair were obtained by DLP technology using a CAD file created from micro-CT of a polyurethane sponge. The idea behind this study was directly inspired by one of the most famous manufacturing strategies currently available for the production of highly porous, trabecular-like scaffolds: the foam replica technique. Open-cell polymeric foams, in fact, have been widely used as sacrificial templates in the

production of bioactive glass and ceramic scaffolds by implementing this versatile and simple strategy, essentially based on the coating of the polymer struts with a layer of glass or ceramic particles.[17,32-35] However, this technique suffers from important shortcomings which limit the industrial scale-up of the process and the spread of foam-replicated structure in the clinical practice.

To the best of the authors' knowledge, the structure of a polyurethane foam has never been reproduced so far by an additive manufacturing system applied to bioceramics. This was also the first time that micro-CT was coupled with DLP to produce a "2.0 version" of foam-replicated bone-like bioceramic scaffolds.

Despite their delicate structure and high porosity, the green samples were able to withstand the layer-by-layer printing process and no samples crumbled or detached from the building platform before the end of the process (Figure 3A). The size, geometry and porous architecture of the green bodies were not apparently damaged by the cleaning process (Figure 3B), which was carried out very cautiously due to the thinness of the struts (Figure 3C). The as-printed samples (the so-called green bodies) initially exhibited a gray-white appearance and then changed colour to light blue after sintering (Figure 3D). This is a normal chromatic effect in sintered hydroxyapatite, which was also observed in some commercial products (eg, Bio-Eye® porous hydroxyapatite orbital implant): negligible traces of manganese can change the hydroxyapatite color to blue after sintering at high temperature in oxidizing atmosphere as a result of the oxidation of manganese ions within the crystalline lattice of hydroxyapatite.[36]

Preliminary tests revealed a shrinkage of ~17% in xy direction and ~19% in z direction after sintering. Overall, the sample shrinkage was low and almost uniform in all the spatial directions as compared to the results reported in other studies on DLP-based grid-like hydroxyapatite scaffolds, which exhibited heterogeneous and higher shrinkage (~36% in xy direction vs. ~14% in z direction) in spite of being sintered at lower temperature (1200°C for 2 hours).[37] This suggests that there was no direction undergoing more stress than another one in the samples sintered in the present work. The application of shrinkage compensation factors yielded final dimensions of the scaffolds very close to the nominal ones, as alredy reported in the Section 2.2.

XRD analysis performed on sintered scaffolds (Figure 4) confirmed the presence of hydroxyapatite as the unique crystalline phase; the JCPDS code for such phase (00-009-0432) is the same found by other authors who fabricated grid-like scaffolds by DLP-based stereolithography.[37] Neither impurities (eg, CaO) nor secondary calcium phosphate phases were detected unlike in the article by Zeng et al.,[37] who reported the conversion of small fractions of hydroxyapatite to both β- and α-tricalcium phosphate (TCP) upon sintering above 1200°C. The stability of
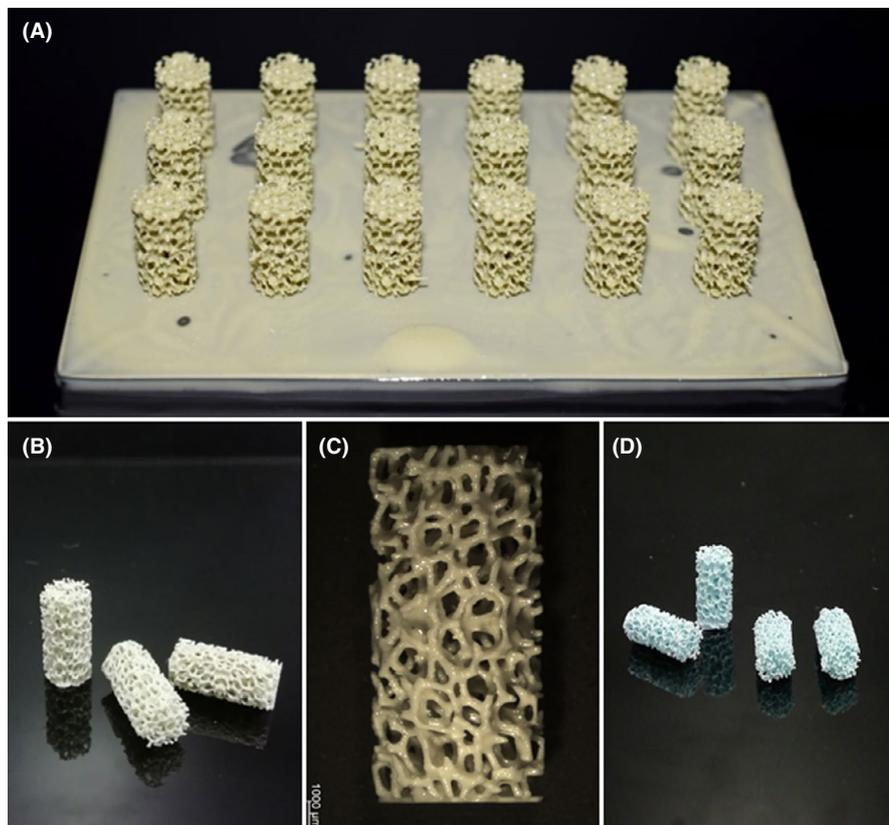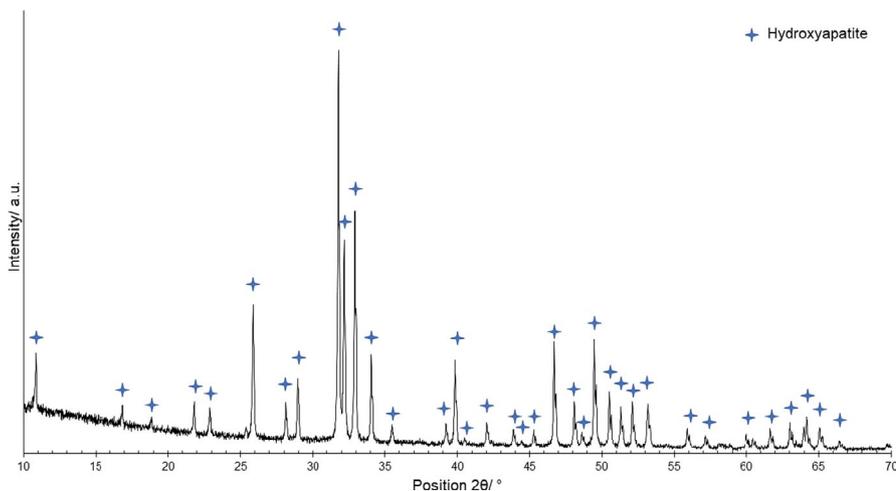
hydroxyapatite phase in our scaffolds could be justified by the high-quality of the starting materials (Ca-to-P weight ratio of 2.35 with 99.9% purity according to the test certificate, as assessed by Rietveld calculation), which was shown to play a role in inhibiting the phase transformation of hydroxyapatite during sintering.[38]

Morphological investigations shown in Figure 5A,B confirm that the 3D pore-strut architecture of the scaffolds closely reproduces the cellular structure of the starting polymeric template (virtual model) and mimics the trabecular organization of cancellous bone. The macropore size is in the range of 100 to 800 μm, which is optimal to allow diffusion of nutrients/removal of waste byproducts, bone cell colonization, blood vessel infiltration and new bone regeneration.[39-41]

Struts are approximately round-shaped with diameter of about 259 ± 30 μm, well-densified (Figure 5C) and without any macroscopic defects, suggesting a successful sintering of the scaffold. Surface microporosity deriving from interparticle voids (Figure 5D) can be beneficial to promote the adhesion of osteoblasts to the scaffold struts.[42]

The total porosity of sintered hydroxyapatite scaffolds was 0.80 ± 0.020, which is comparable to the typical range of healthy human cancellous bone (0.50-0.85[43-45]) and, therefore, suggests a potential suitability for bone substitution. The low value of standard deviation for scaffold porosity
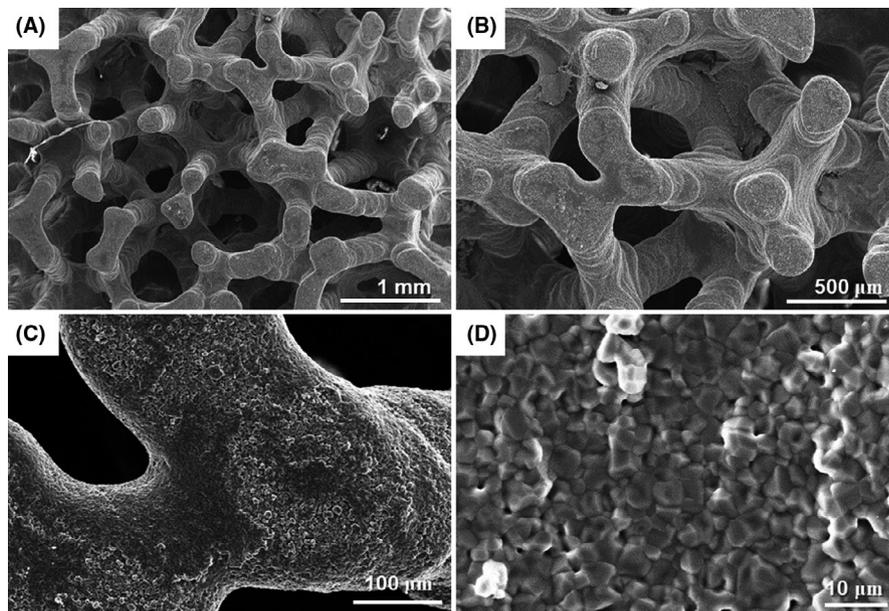
also indicates a good reproducibility of the manufacturing process.

Dealing with scaffolds for bone tissue engineering applications, an accurate determination of intrinsic permeability is crucial to predict scaffold performances in the physiological environment. Intrinsic permeability, in fact, characterizes both scaffold architecture and mass-transport properties, and hence quantifies the ability of a porous material to conduct fluid flow through its whole volume. When a 3D bone scaffold is implanted, proper mass transport has to be guaranteed to promote cell migration from the periphery to the internal core and favor nutrient/oxygen supply and catabolite elimination, thus improving the quality of the final tissue.[46] The intrinsic permeability of the hydroxyapatite scaffolds is in the range of 0.75 to 1.74×10^{-9} m^2, which is comparable to the lower ranges determined for human cancellous bone harvested from calcaneus ($0.4\text{-}11.0 \times 10^{-9}$ m^2 [47]) and vertebral body ($1.5\text{-}12.1 \times 10^{-9}$ m^2 [46]); a closer similarity was observed with bone from proximal femur ($0.01\text{-}4.7 \times 10^{-9}$ m^2 [46]). Scaffold permeability could be further optimized by refining the 3D model in the CAD file used for printing (e.g., adjustment of strut diameter/pore size). For the sake of comparison, it is interesting to mention that the intrinsic permeability of commercial clinically used calcium carbonate scaffolds, analysed under the same experimental setup (acoustic method), was two orders of magnitude lower (around 3.12×10^{-11} m^2).[24] This further demonstrates that the overall strategy used to fabricate hydroxyapatite scaffolds (micro-CT combined with DLP-based stereolithography) has the potential to lead to an improvement over the scientific, commercial and clinical state of the art and to developing porous biomaterials with bone-like architecture and mass transport properties.

The compressive strength of scaffolds as such and after immersion in SBF for 2 weeks and 1 month was 1.60 ± 0.79, 1.28 ± 0.32, and 1.54 ± 0.36 MPa, respectively. All these values within the typical range of trabecular bone ($0.1\text{-}16$ MPa [48,49]), although being close to the lower limit. Prolonged immersion in SBF did not lead to any significant variation in the mechanical strength of scaffolds; this can be justified by the fact that hydroxyapatite a very slow resorption rate in biological fluids, unless in the form of nanoparticles.[50] These values are from 4 to 8 times higher than those obtained for hydroxyapatite scaffolds ($0.21\text{-}0.41$ MPa) having analogous total porosity ($0.82\text{-}0.86$) and fabricated by conventional sponge replication.[51] Another study revealed that the use of nano-sized hydroxyapatite particles (diameter around 150 nm) to coat the polyurethane sponge in the conventional method yielded no significant improvement in the compressive strength (0.51 MPa).[8] This suggests that, although the same template (polyurethane sponge) is used in both DLP-based stereolithography (as a virtual model in the present work) and conventional foam replication, the production method indeed plays a key role in affecting the mechanical performance of scaffolds and, thus, their clinical suitability for bone repair.

Grid-like hydroxyapatite scaffolds produced by DLP-based stereolithography and sintered under analogous conditions than the present trabecular samples exhibited comparable compressive strength ($1.45\text{-}1.92$ MPa) but, surprisingly, markedly lower porosity ($0.49\text{-}0.52$) around the minimum threshold for cancellous bone.[52]

A typical stress-strain curve obtained upon compression is depicted in Figure 6.

The elastic modulus of scaffolds, 513 ± 290 MPa, is comparable to the reference range for cancellous bone
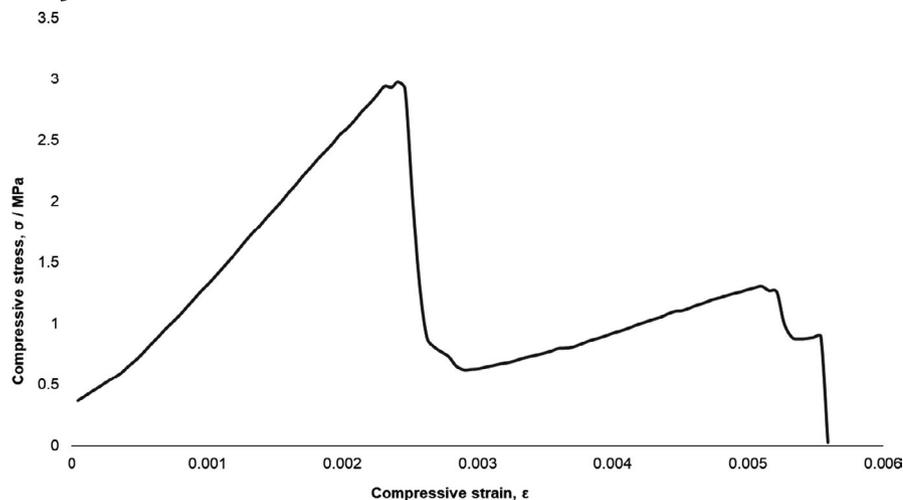
FIGURE 6 Representative stress-strain curve obtained upon compressive mechanical tests
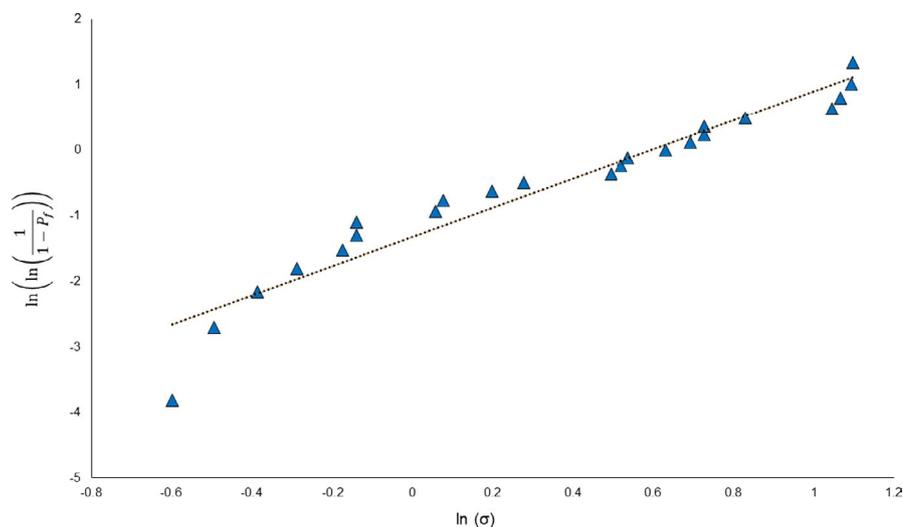

FIGURE 7 Weibull plot with linear fitting for the compressive strength of DLP-derived hydroxyapatite scaffolds

(50-500 MPa [53,54]) this is an important result to avoid stiffness mismatch between implanted biomaterial and host bone.

Figure 7 shows the Weibull plot of the compressive strength data; least mean squares fitting of a straight line through the experimental points yields Weibull modulus $m = 2.2$ and Weibull scale parameter $\sigma_0 = 1.81$ MPa, corresponding to the stress value at which 63% of the specimens are expected to survive. The Weibull modulus determined from the strength data for a large number of theoretically identical samples (more than 20) provides a measure of the mechanical reliability of brittle materials, like ceramics. The mechanical response of brittle materials is sensitive to microstructural flaws such as pores and micro-cracks: therefore, Weibull modulus is used to evaluate the probability of failure in such materials under a given stress. This parameter was seldom determined for bioceramic scaffolds in the literature; the Weibull modulus of robocast hydroxyapatite, β-TCP and calcium polyphosphate scaffolds has been reported to be in the range of 3.2 (perpendicular to ceramic rods) to 9.9 (parallel to ceramic rods) upon testing in compression,[11,55] and an improvement from 3.0 to 7.7

could be achieved by applying a polymeric coating (poly(-lactic acid) and poly(ε-caprolactone)) on β-TCP structures.[56] Furthermore, β-TCP scaffolds produced by DLP exhibited a Weibull modulus ranging from 3.2 to 7.4 depending on the architectural geometry (eg, grid-like and hexagonal).[20] However, all these calcium phosphate scaffolds had a less porous, ordered structure of parallel/perpendicular rods instead of a highly porous foam-like architecture, like that of the hydroxyapatite scaffolds produced in this work; such a difference could explain the relatively low value of Weibull modulus in the latter case.

The fabrication approach followed in this work, relying on the "ceramic replication" of a polymeric sponge by DLP-based stereolithography, allows obtaining standardized scaffolds with high control on pore/strut characteristics, good reproducibility, appealing market potential and higher mechanical strength compared to conventional sponge replication. Indeed, some degrees of freedom in scaffold design are still possible by properly processing the starting CAD file (volumetric reconstruction) from micro-CT imaging. In this work, thickening of 25 μm was applied to the sponge struts but other options are possible on

demand: the proposed fabrication platform is potentially suitable for both mass production and customization of scaffolds (personalized medicine), if necessary.

4 | SUMMARY

It has been shown, for the first time, that porous bioceramics can be produced by DLP-based stereolithography using a micro-CT reconstruction of an open-cell polymeric foam as a virtual template (CAD model). As a result, it was possible to fabricate hydroxyapatite scaffolds with 3D trabecular architecture, pore size, intrinsic permeability, elastic modulus, and compressive strength comparable to those of human cancellous bone. This novel approach opens new horizons in the functional design and manufacturing of bone-like scaffolds that could be highly beneficial in bone replacement and bone tissue engineering strategies.

ORCID

Francesco Baino https://orcid.org/0000-0001-8860-0497
Martin Schwentenwein https://orcid.org/0000-0002-2076-5575
Enrica Verné https://orcid.org/0000-0002-8649-4739

REFERENCES

1. Maraldi T, Riccio M, Pisciotta A, Zavatti M, Carnevale G, Beretti F, et al. Human amniotic fluid-derived and dental pulp-derived stem cells seeded into collagen scaffold repair critical-size bone defects promoting vascularization. Stem Cell Res Ther. 2013;4(3):1.
2. Campana V, Milano G, Pagano E, Barba M, Cicione C, Salonna G, et al. Bone substitutes in orthopaedic surgery: from basic science to clinical practice. J Mater Sci Mater Med. 2014;25(10):2445–61.
3. Hutmacher DW, Schantz JT, Lam CXF, Tan KC, Lim TC. State of the art and future directions of scaffold-based bone engineering from biomaterials perspective. J Tissue Eng Regen Med. 2007;1(4):245–60.
4. Pina S, Ribeiro VP, Marques CF, Maia FR, Silva TH, Reis RL, et al. Scaffolding strategies for tissue engineering and regenerative medicine applications. Materials (Basel). 2019;12(11).
5. Boskey AL. Mineralization of bones and teeth. Elements. 2007;3(6):385–91.
6. Dorozhkin SV, Epple M. Biological and medical significance of calcium phosphates. Angew Chemie - Int Ed. 2002;41(17):3130–46.
7. Oliveira JM, Silva SS, Malafaya PB, Rodrigues MT, Kotobuki N, Hirose M, et al. Macroporous hydroxyapatite scaffolds for bone tissue engineering applications: physicochemical characterization and assessment of rat bone marrow stromal cell viability. J Biomed Mater Res A. 2009;91(1):175–86.
8. Gervaso F, Scalera F, Kunjalukkal Padmanabhan S, Sannino A, Licciulli A. High performace hydroxyapatite scaffolds for bone tissue engineering applications. Int J Appl Ceram Technol. 2012;9(3):507–16.
9. Andrade JCT, Camilli JA, Kawachi EY, Bertran CA. Behavior of dense and porous hydroxyapatite implants and tissue response in rat femoral defects. J Biomed Mater Res. 2002;62(1):30–6.
10. Tadic D, Beckmann F, Schwarz K, Epple M. A novel method to produce hydroxyapatite objects with interconnecting porosity that avoids sintering. Biomaterials. 2004;25(16):3335–40.
11. Miranda P, Pajares A, Saiz E, Tomsia AP, Guiberteau F. Mechanical properties of calcium phosphate scaffolds fabricated by robocasting. J Biomed Mater res A. 2008;85(1):218–27.
12. Kumar A, Kargozar S, Baino F, Han SS. Additive manufacturing methods for producing hydroxyapatite and hydroxyapatite-based composite scaffolds: a review. Front Mater. 2019;6:1–20.
13. Potestio I. Lithoz: how lithography-based ceramic AM is expanding the opportunities for technical ceramics. Powder Inject Mould Int. 2019;13(2):2–5.
14. Felzmann R, Gruber S, Mitteramskogler G, Tesavibul P, Boccaccini AR, Liska R, et al. Lithography-based additive manufacturing of cellular ceramic structures. Adv Eng Mater. 2012;14(12):1052–8.
15. Baino F, Fiume E, Barberi J, Kargozar S, Marchi J, Massera J, et al. Processing methods for making porous bioactive glass-based scaffolds—A state-of-the-art review. Int J Appl Ceram Technol. 2019;16(5):1762–96.
16. Lantada AD, De Blas RA, Schwentenwein M, Jellinek C, Homa J. Lithography-based ceramic manufacture (LCM) of auxetic structures: present capabilities and challenges. Smart Mater Struct. 2016;25(5).
17. Baino F, Caddeo S, Novajra G, Vitale-Brovarone C. Using porous bioceramic scaffolds to model healthy and osteoporotic bone. J Eur Ceram Soc. 2016;36(9):2175–82.
18. Junqueira Amorim PH, De Moraes TF, De Souza Azevedo F, Cunha Peres AS, De Oliveira e Souza VH, Matsuda RH, et al. InVesalius User guide. 2007. p. 130. ftp://ftp.cti.gov.br/pub/dt3d/invesalius/files/user_guide_en_v3.1.1.pdf. Accessed 14 Apr 2021.
19. Hing KA, Best SM, Bonfield W. Characterization of porous hydroxyapatite. J Mater Sci Mater Med. 1999;10(3):135–45.
20. Schmidleithner C, Malferrari S, Palgrave R, Bomze D, Schwentenwein M, Kalaskar DM. Application of high resolution DLP stereolithography for fabrication of tricalcium phosphate scaffolds for bone regeneration. Biomed Mater. 2019;14(4):045018.
21. Hubbert MK. Darcy's law and the field equations of the flow of underground fluids. Hydrol Sci J. 1957;2(1):23–59.
22. Whitaker S. Flow in porous media I: a theoretical derivation of Darcy's law. Transp Porous Media. 1986;1:3–25.
23. Lasseux D, Valdés-Parada FJ. On the developments of Darcy's law to include inertial and slip effects. Comptes Rendus Mécanique. 2017;345(9):660–9.
24. Schiavi A, Guglielmone C, Pennella F, Morbiducci U. Acoustic method for permeability measurement of tissue-engineering scaffold. Meas Sci Technol. 2012;23:105702.
25. Pennella F, Cerino G, Massai D, Gallo D, Falvo D'Urso Labate G, Schiavi A, et al. A survey of methods for the evaluation of tissue engineering scaffold permeability. Ann Biomed Eng. 2013;41(10):2027–41.
26. Fiume E, Schiavi A, Orlygsson G, Bignardi C, Verné E, Baino F. Comprehensive assessment of bioactive glass and glass-ceramic scaffold permeability: experimental measurements by pressure wave drop, modelling and computed tomography-based analysis. Acta Biomater. 2021;119:405–18.
27. Chor MV, Li W. A permeability measurement system for tissue engineering scaffolds. Meas Sci Technol. 2017;18:208–16.
28. ASTM C1239-07. Standard practice for reporting uniaxial strength data and estimating Weibull distribution parameters for advanced ceramics.

29. Kokubo T, Takadama H. How useful is SBF in predicting in vivo bone bioactivity? Biomaterials. 2006;27(15):2907–15.

30. Mozafari M, Banijamali S, Baino F, Kargozae S, Hill RG. Calcium carbonate: adored and ignored in bioactivity assessment. Acta Biomater. 2019;91:35–47.

31. Macon ALB, Kim TB, Valliant EM, Goetschius K, Brow RK, Day DE, et al. A unified in vitro evaluation for apatite-forming ability of bioactive glasses and their variants. J Mater Sci Mater Med. 2015;26(2):115.

32. Chen QZ, Thompson ID, Boccaccini AR. 45S5 Bioglass®-derived glass–ceramic scaffolds for bone tissue engineering. Biomaterials. 2006;27(11):2414–25.

33. Vitale-Brovarone C, Baino F, Bretcanu O, Verné E. Foam-like scaffolds for bone tissue engineering based on a novel couple of silicate-phosphate specular glasses: synthesis and properties. J Mater Sci Mater Med. 2009;20:2197–205.

34. Falvo D'Urso Labate G, Catapano G, Vitale-Brovarone C, Baino F. Quantifying the micro-architectural similarity of bioceramic scaffolds to bone. Ceram Int. 2017;43(12):9443–50.

35. Baino F, Fiume E. Mechanical characterization of 45S5 bioactive glass-derived scaffolds. Mater Lett. 2019;245:14–7.

36. Li Y, Klein CPAT, Zhang X, Groot DE. Relationship between the colour change of hydroxyapatite and the trace element manganese. Biomaterials. 1993;14(13):969–72.

37. Zeng Y, Yan Y, Yan H, Li P, Zhao Y, Liu C, et al. 3D printing of hydroxyapatite scaffolds with good mechanical and biocompatible properties by digital light processing. J Mater Sci. 2018;53(9):6291–301.

38. Sanosh KP, Chu MC, Balakrishnan A, Kim TN, Cho SJ. Pressureless sintering of nanocrystalline hydroxyapatite at different temperatures. Met Mater Int. 2010;16(4):605–11.

39. Tsuruga E, Takita H, Itoh H, Wakisaka Y, Kuboki Y. Pore size of porous hydroxyapatite as the cell-substratum controls BMP-induced osteogenesis. J Biochem. 1997;121(2):317–24.

40. Perez RA, Mestres G. Role of pore size and morphology in musculoskeletal tissue regeneration. Mater Sci Eng C. 2016;61:922–39.

41. Legeros RZ. Properties of osteoconductive biomaterials: calcium phosphates. Clin Orthop Relat Res. 2002;395:81–98.

42. Simske SJ, Ayers RA, Bateman TA. Porous materials for bone engineering. Mater Sci Forum. 1997;250:151–82.

43. Hildebrand T, Laib A, Müller R, Dequeker J, Rüegsegger P. Direct three-dimensional morphometric analysis of human cancellous bone: microstructural data from spine, femour, iliac crest, and calcaneus. J Bone Miner Res. 1999;14(7):1167–74.

44. Link TM, Vieth V, Langenberg R, Meier N, Lotter A, Newitt D, et al. Structure analysis of high resolution magnetic resonance imaging of the proximal femur: in vitro correlation with biomechanical strength and BMD. Calcif Tissue Int. 2003;72(2):156–65.

45. Krug R, Banerjee S, Han ET, Newitt DC, Link TM, Majumdar S. Feasibility of in vivo structural analysis of high-resolution magnetic resonance images of the proximal femur. Osteoporos Int. 2005;16(11):1307–14.

46. Nauman EA, Fong KE, Keaveny TM. Dependence of intertrabecular permeability on flow direction and anatomic site. Ann Biomed Eng. 1999;27(4):517–24.

47. Grimm MJ, Williams JL. Measurements of permeability in human calcaneal trabecular bone. J Biomech. 1997;30:743–5.

48. Keaveny TM, Morgan EF, Niebur GL, Yeh OC. Biomechanics of trabecular bone. Annu Rev Biomed Eng. 2001;3:307–33.

49. Keller TS, Carter DR, Hernandez CJ, Beaupre GS. The influence of bone volume fraction and ash fraction on bone strength and modulus. Bone. 2001;29(1):74–8.

50. Barrere F, Van Blitterswiik CA, De Groot K. Bone regeneration: molecular and cellular interactions with calcium phosphate ceramics. Int J Nanomed. 2006;1:317–32.

51. Kim HW, Knowles JC, Kim HE. Hydroxyapatite porous scaffold engineered with biological polymer hybrid coating for antibiotic Vancomycin release. J Mater Sci Mater Med. 2005;16(3):189–95.

52. Feng C, Zang K, He R, Ding G, Xia M. Additive manufacturing of hydroxyapatite bioceramic scaffolds: dispersion, digital light processing, sintering, mechanical properties, and biocompatibility. J Adv Ceram. 2020;9(3):360–73.

53. Thompson ID, Hench LL. Mechanical properties of bioactive glasses, glass-ceramics and composites. Proc Inst Mech Eng H. 1998;212:127–37.

54. Kaur G, Kumar V, Baino F, Mauro JC, Pickrell G, Evans I, et al. Mechanical properties of bioactive glasses, ceramics, glass-ceramics and composites: state-of-the-art review and future challenges. Mater Sci Eng C. 2019;104:109895.

55. Shanjani Y, Hu Y, Pilliar RM, Toyserkani E. Mechanical characteristics of solid-freeform-fabricated porous calcium polyphosphate structures with oriented stacked layers. Acta Biomater. 2011;7(4):1788–96.

56. Martínez-Vázquez FJ, Perera FH, Miranda P, Pajares A, Guiberteau F. Improving the compressive strength of bioceramic robocast scaffolds by polymer infiltration. Acta Biomater. 2010;6(11):4361–8.